Progress In Electromagnetics Research C, Vol. 60, 47–56, 2015

Four-Element Dual-Band MIMO Antenna System for Mobile Phones

Lingsheng Yang*, Hongling Xu, Jianping Fang, and Tao Li

Abstract—A dual-band multiple-input-multiple-output (MIMO) antenna system for LTE 700/2300/2500, UMTS2100, GSM 1800/1900 mobile phone applications is presented. The whole system consists of four identical 3-D IFAs (inverted F antenna) loaded with lumped inductors and folded on FR4 cuboids. Without any special designed decoupling structures, the measured isolation among antenna elements is higher than 13 dB. Return loss characteristics, correlation coefficient, gain and radiation performance are also presented.

1. INTRODUCTION

With the rapid development of wireless communications systems, the fourth long-term evolution (LTE) communication system has been widely applied, and MIMO becomes a key technology since it can increase the channel capacity without extra radiation power and spectrum bandwidth. According to [1], the channel capacity can increase directly proportional to the number of transmitter and receiver antennas within a multipath environment. However, for mobile phones, when the number of elements increases, the valuable size becomes a major limitation. The designed antenna should be small in size and can cover more operating bands, such as GSM1800/1900 (1710–1880 MHz/1850–1990 MHz) used for second generation wireless communication, UMTS2100 (1920–2170 MHz) for third generation and the new operational bands LTE700/2300/2500 (758–798 MHz/2305–2400 MHz/2500–2690 MHz) for fourth long-term evolution (LTE) communication system. 3-D IFAs are good candidates and were used in [2–4] due to their lower Q and wide bandwidth characteristics. Considering the relatively long wavelength for frequency lower than GHz, lumped inductors were loaded with antenna element to obtain 0.25-wavelength resonant mode with a smaller size [5, 6].

Besides the need of wide operating bandwidth and small size, for MIMO system design, how to maintain a high isolation among antenna elements is another big challenge, since in most instances the space between antenna elements is smaller than a half wavelength. In [2], by carefully designing the length, width and insert position of a suspended neutralization line, isolation in the LTE13 band and 2.61–2.84 GHz band can be improved. Inverted-L branches and a rectangular slot etched on the ground plane were used in [7, 8], and in order to obtain sufficient decoupling effect, the slots are longer than 40 mm. In [9], T-shaped common radiator acted as the decoupling element to obtain high isolation (> 17 dB) for LTE 13 (746–787) band. In [10], besides T-shaped ground branch, the antenna elements were arranged orthogonally to achieve high isolation in both lower than GHz and higher than GHz band.

In this paper, we present a compact four-element MIMO antenna system. By using lumped inductor loaded 3-D folded IFA as the element, the whole system has two measured -6 dB impedance bands of 70 MHz (740–810 MHz) and 1010 MHz (1.69–2.70 GHz) with a size of 140 mm $\times$ 70 mm $\times$ 6 mm. The proposed four-antenna system does not need any special designed decoupling structures, while higher than 13 dB isolation in both operating bands can be obtained. In the LTE700 band higher than 20 dB, measured isolation can be achieved.

Received 13 October 2015, Accepted 18 November 2015, Scheduled 30 November 2015

* Corresponding author: Lingsheng Yang (ylsinchina@163.com).

The authors are with the Jiangsu Key Laboratory of Meteorological Observation and Information Processing & Research Center of Applied Electromagnetics of NUIST, Nanjing University of Information Science & Technology, NingLiu Road, Nanjing 210044, China.

2. MIMO ANTENNA DESIGN

The proposed four-element MIMO antenna system is shown in Fig. 1. Four 3-D IFAs are mounted on the top layer of a 140 mm × 70 mm × 1 mm FR4 substrate, with relative permittivity of 4.4 and loss tangent of 0.02. The bottom layer of the substrate is copper and works as the common ground plane while the four corners are with 15 mm × 19 mm cut respectively. Four L-shaped stubs are connected with the ground plane just under the IFAs. The comparison between the proposed system and recently published papers for size and bandwidth is listed in Table 1. By comparison, the proposed antenna has a compact size and acceptable bandwidth performances.

The geometry of the dual-band antenna element is shown in Figs. 2(a) and (b). HFSS (ver.15) was used to optimize the topology of the antenna. The IFA is loaded with two lumped inductors (red 2.4 nH, green 9.1 nH) and is designed to have an electrical length approximately equal to 0.25-wavelength at the center of the frequency bands as LTE14 (770 MHz), GSM1900 (1.9 GHz), and LTE2500 (2.58 GHz) with a compact antenna size 15 mm × 15 mm × 5 mm. In the simulation, we only use a simple inductor to simulate the real inductors. The inductor is loaded on the strip where the strongest current intensity

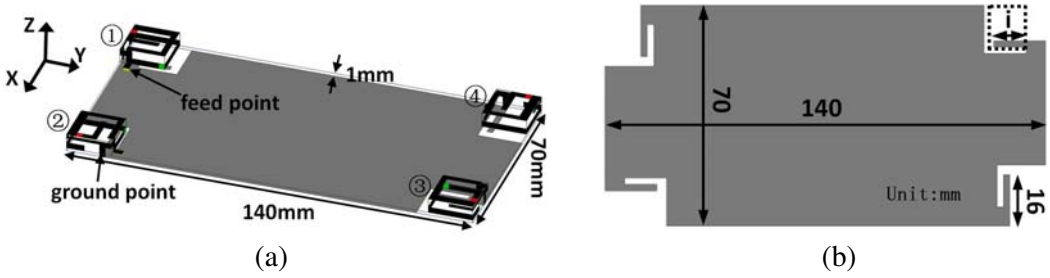

Figure 1. (a) Geometry of the 4-element MIMO antenna system, (b) bottom layer of the substrate.

Table 1. Comparison between the proposed antenna element and the recently published antennas.

Antennas	Size	Bands (MHz)
proposed	15 × 15 × 5	740–810, 1690–2700
[2]	15 × 15.2 × 7.2	748–785, 2610–2840
[5]	15 × 40 × 4	698–960, 1710–2690
[9]	60 × 15 × 5	746–787
[14]	25 × 10 × 5	700–960

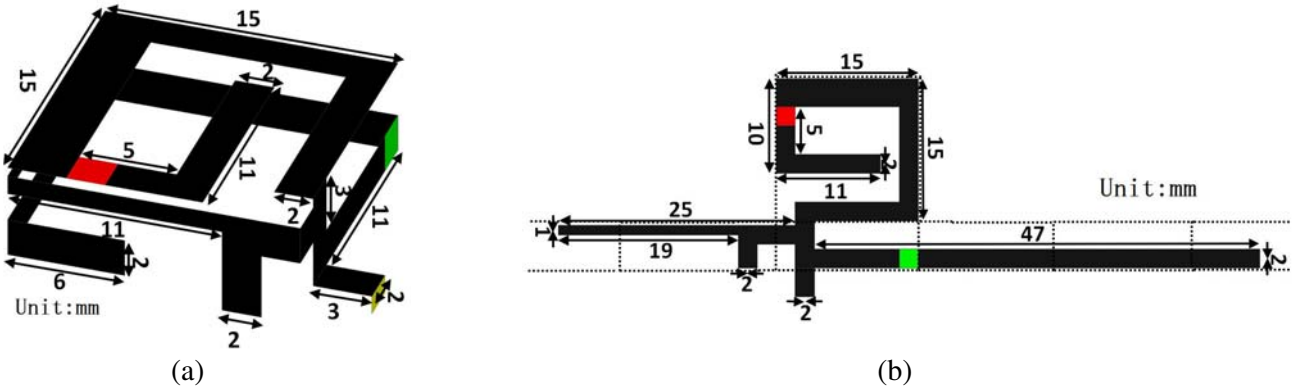

Figure 2. Configuration of the tri-band antenna, (a) element#1, (b) unfolded figure of element#1.

occurs. The final locations are the optimized results of the simulation. The yellow rectangular is the lumped port used in simulation connecting the radiation element and the ground through the substrate.

The simulated reflection coefficient characteristics of the antenna are plotted in Figs. 3(a) and (b). The input impedance on the Smith Chart in the second band is shown in Fig. 3(c). In the wide band (1.5–2.7 GHz), the antenna is well matched, and the VSWR is less than 3. For frequency at around 2.42 GHz, the input impedance is nearly 50 ohm, while for frequency at around 2.36 GHz, the impedance is not well matched compared with other frequencies.

The design process of the antenna is analyzed. As shown in Fig. 4(a), without strip **#a**, the resonance frequency at around 760 MHz disappears. Only with strip **#b**, resonance frequency can be obtained at around 1.1 GHz, and the strip **#a** can prolong strip **#b** and shift the 1.1 GHz resonance frequency to 760 MHz. When strip **#c** is added to strip **#a**, another resonance frequency at 790 MHz can be fulfilled. The two adjacent resonance frequencies form a wider than 40 MHz bandwidth. Meanwhile, strip **#a, #b** and **#c** can form a second band about 1.51–2.4 GHz. When L-shaped strip is added, the second bandwidth can be widened to 2.75 GHz, and the reflection coefficients can also be improved in the first band. The antenna bandwidth with the change of the L-shaped strip is further shown in Fig. 4(b). For the first band, the influence mainly occurs in the middle of the band, while for the second

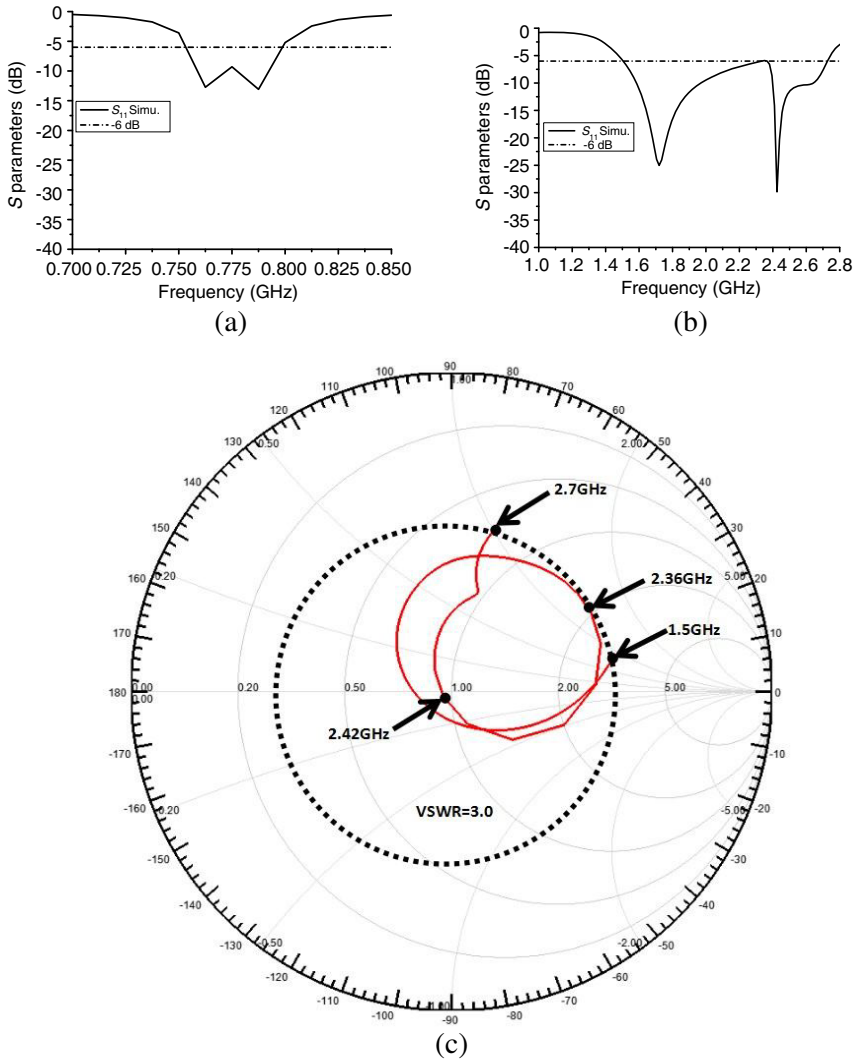

Figure 3. Simulated antenna reflection coefficient characteristics (a) lower band, (b) higher band, (c) simulated input impedance on Smith Chart in the frequency range of 1.5–2.7 GHz.

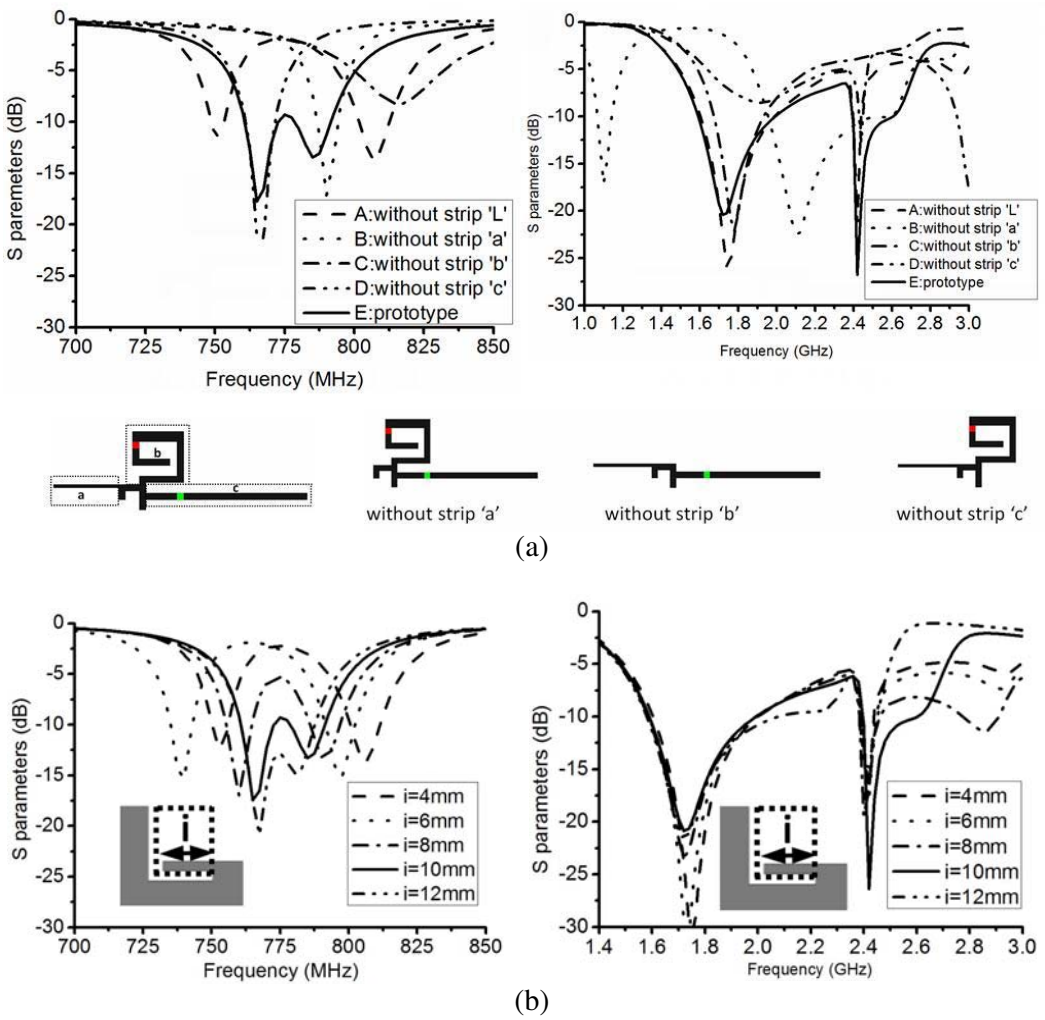

Figure 4. (a) Comparison between the simulated reflection coefficient of the prototype antenna and three antennas for reference, (b) reflection coefficient characteristics of the antenna with the change of the length of the L-shaped strip.

band, higher than 2.4 GHz band is mainly affected.

The surface current distributions on the antenna element can further explain the functions of different parts of the antenna element. In Fig. 5(a), the current flows on strip **#a** and strip **#b**, together with the 2.4 nH inductor, and a resonance of 760 MHz can be obtained. On the other hand, in Fig. 5(b), the current distributes on strip **#c**, with the 9.1 nH inductor, a resonance of 790 MHz can be achieved. The two aforementioned current paths together form the first band. As shown in Fig. 5(c), the current length on strip **#a** is around 24 mm, 0.25-wavelength at 1.9 GHz, while the higher than 2 GHz part of the second band is a joint action of all three strips (Fig. 4(a)). Also can be seen in Fig. 5, currents distribute on the L-shaped strip too, which explains that the L-shaped strip couples with the antenna and affects the bandwidth performances.

The current distributions on the whole PCB board is plotted in Fig. 5(e), at the lower band frequency, the surface current is distributed mainly in the vicinity of the antenna element. On the other hand, at the lower frequency part of the higher band (around 1.7–2.4 GHz), the currents spread to other elements. When the frequency becomes higher (about 2.4–2.7 GHz), the currents concentrate on the antenna element again. These current distribution performances coincide with the isolation performances of the MIMO system.

When the number of elements increases, size becomes a major limitation, and the conventional

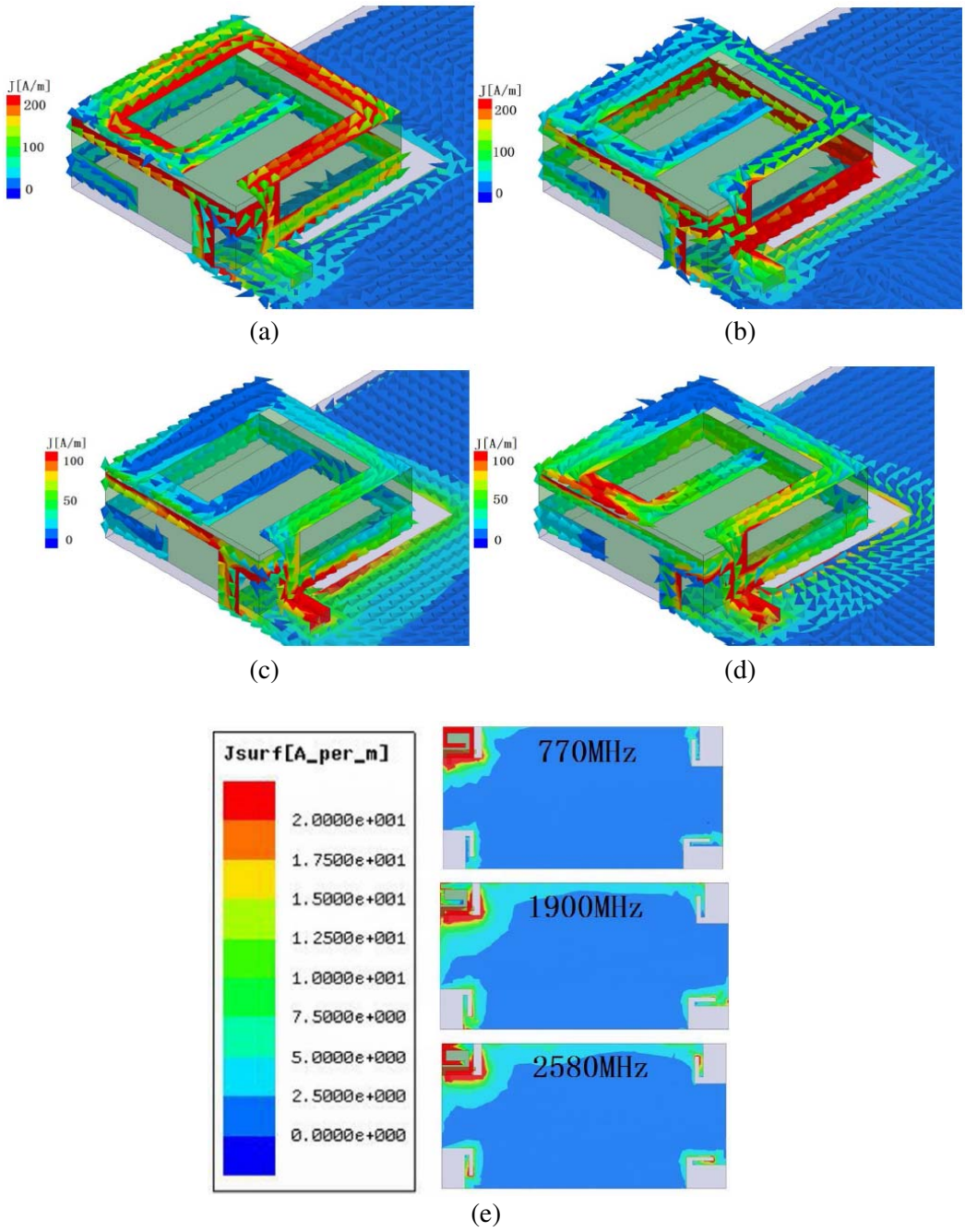

Figure 5. Surface current distributions at (a) 760 MHz and (b) 790 MHz, (c) 1.9 GHz and (d) 2.58 GHz, (e) surface current distributions on the whole PCB board.

methods such as applying decoupling structures between antenna elements and arranging the antenna elements at different positions of the mobile handset to improve the isolation become invalid. Since the antenna element proposed in this paper has a 3D structure and can be rotated freely, we can use different orientations of the antenna to change the radiation characteristics of the antenna element hence improve the isolation between antenna elements.

In order to obtain a high isolation among antenna elements, the strongest radiation of the element should not be oriented to the nearest element or other two elements, or the strongest radiation should be oriented to the null radiation of another antenna elements. Taking the strip connected to the feed

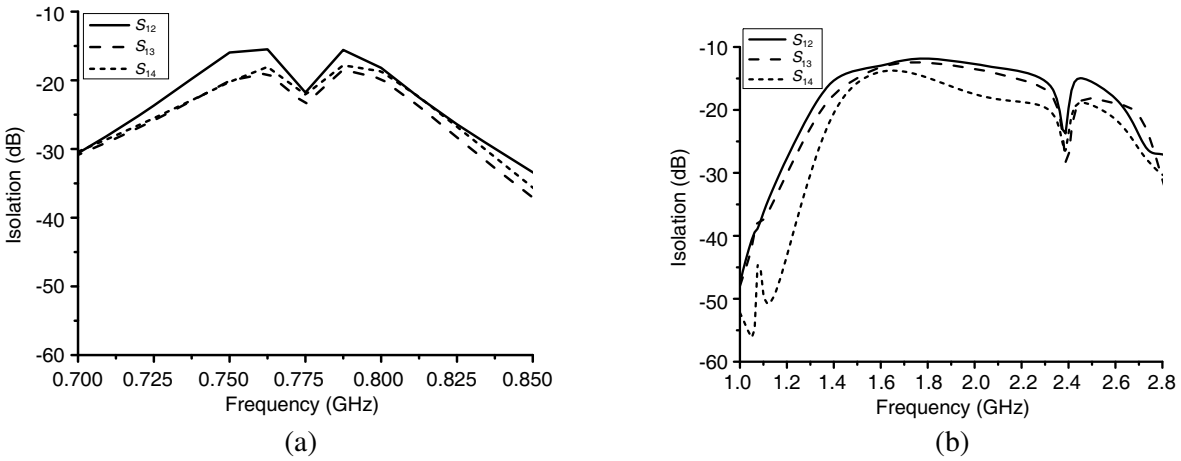

Figure 6. Simulated isolation (a) lower band, (b) higher band (to this end see Fig. 1(a)).

point (yellow part in Fig. 2(a)) as the needle, the elements in Fig. 1 can be seen as orthogonal to each other. The simulated isolation of the MIMO system is shown in Fig. 6, higher than 15 dB isolation in the first band, and no less than 13 dB isolation in the second band can be obtained.

3. RESULTS AND DISCUSSION

3.1. Measured Results

A photograph of the fabricated MIMO antenna system is shown in Fig. 7. The system was measured by using Agilent 85058E vector network analyzer.

Figure 7. Photograph of the fabricated antenna (top and bottom).

Figure 8 shows the measured and simulated return loss characteristics of element#1. Other antennas are not shown here for the sake of clarity. The antenna has two simulated bands 750–799 MHz (49 MHz), and 1.51–2.75 GHz (1240 MHz). On the other hand, the measured 6 dB return loss bands are 740–810 MHz (70 MHz) and 1.69–2.70 GHz (1010 MHz). The differences between the measured and simulated values are probably caused by the size errors during fabrication and the change of performances of the lumped inductors in the higher than GHz band.

The measured isolation among antenna elements is shown in Fig. 9. Higher than 13 dB isolation can be obtained in both the working bands, while higher than 20 dB isolation is achieved at the LTE700 band.

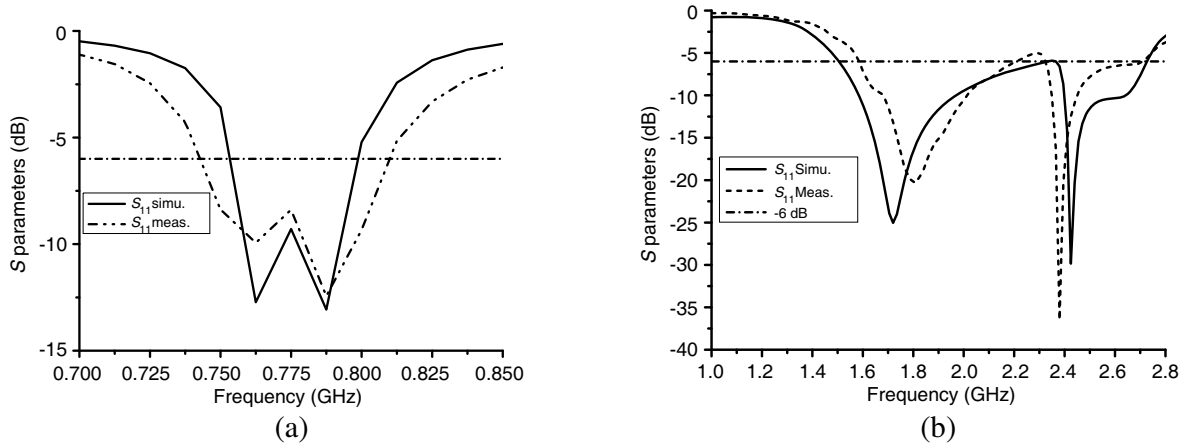

Figure 8. Reflection coefficients of the MIMO antenna system (a) lower band, (b) higher band.

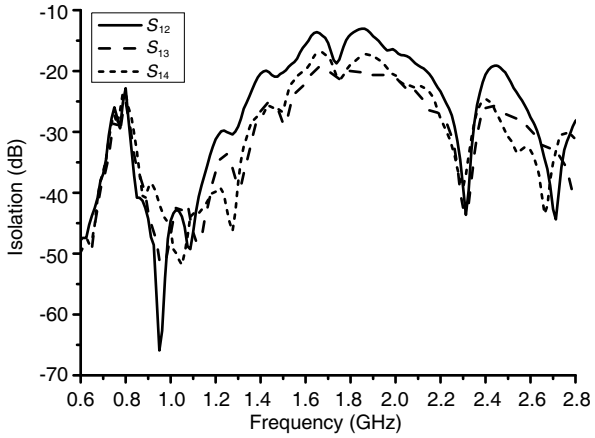

Figure 9. Measured isolation between MIMO antenna elements..

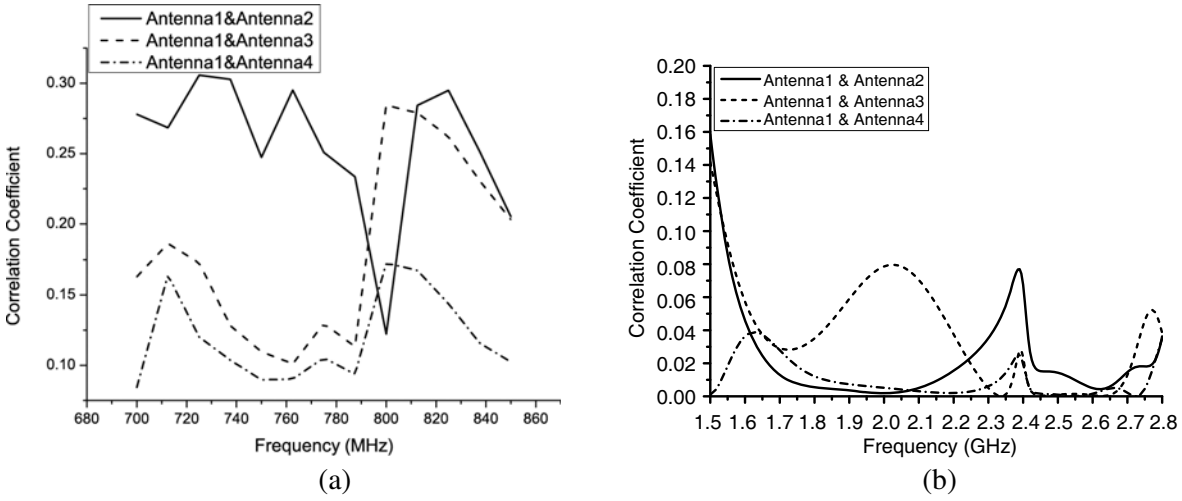

Figure 10. Correlation coefficient curves for the three bands of the proposed MIMO antenna system (a) lower band, (b) higher band.

The correlation coefficient can be used to evaluate the diversity capability of the MIMO system. By using the measured S parameters and the method introduced in [11], the correlation coefficient between the antenna elements can be calculated and is shown in Fig. 10. The maximum value of the correlation coefficient was smaller than the recommended value (0.5) set for 4G standards [12, 13].

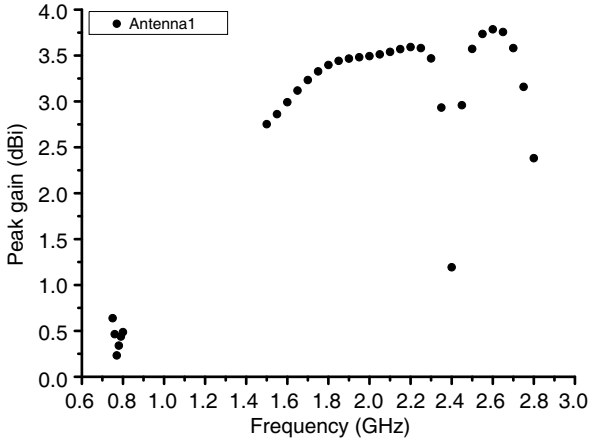

Figure 11. Gain of the proposed antenna.

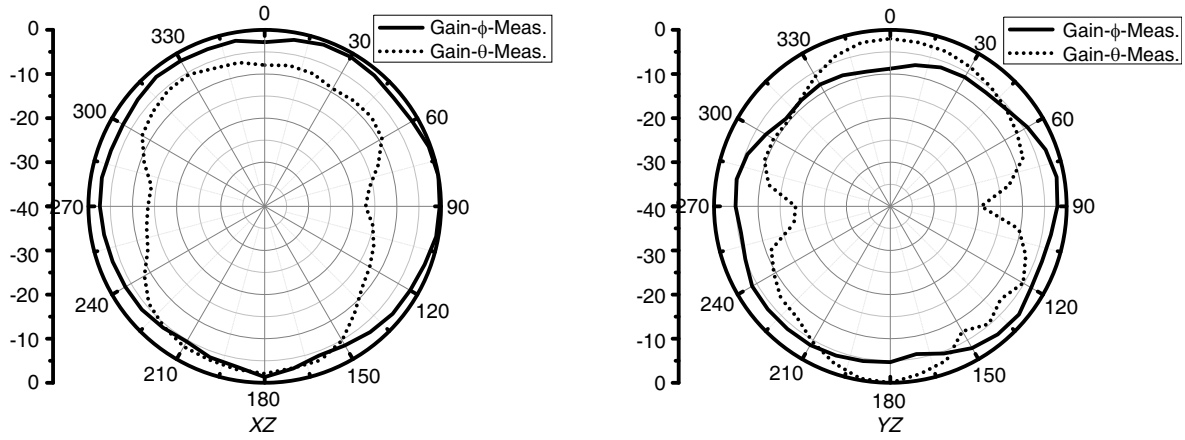

(a)

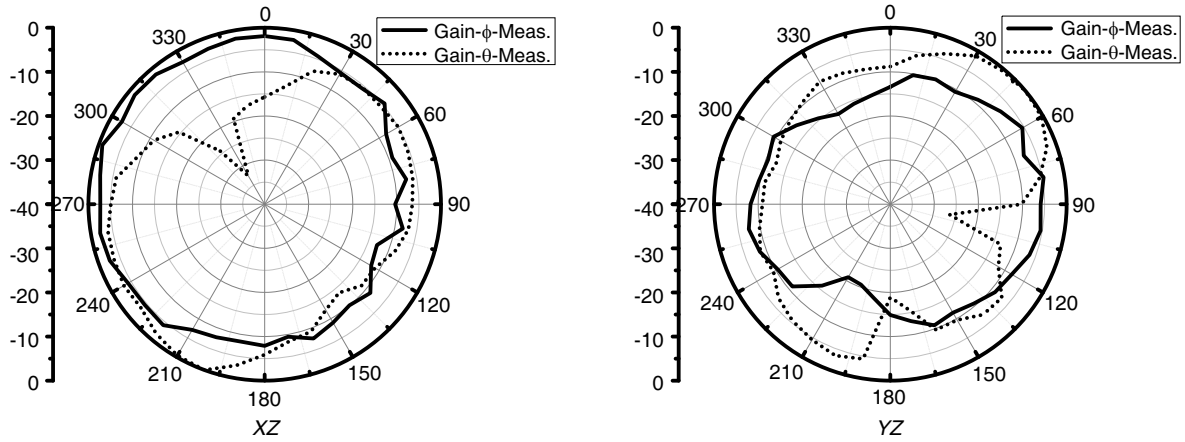

(b)

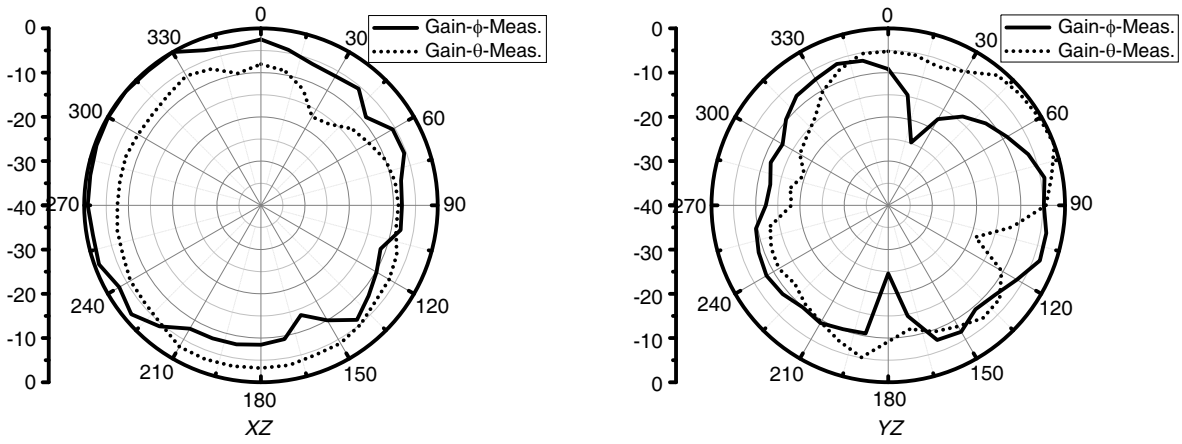

Figure 12. Measured radiation patterns of the proposed antenna: (a) 77 MHz, (b) 1.9 GHz, (c) 2.58 GHz.

The gain versus frequency is plotted in Fig. 11. The gain varies from 0.23–0.64 dBi in the lower band and 1.19–3.79 dBi in the higher band. The simulated antenna efficiency in the lower and higher bands are, respectively, about 38–42% and 65–77%.

The measured radiation patterns of antenna element #1 in xz- and yz-planes at 770 MHz, 1.9 GHz and 2.58 GHz are shown in Fig. 12, and the radiation patterns of element #1 were measured while the other three antenna elements were terminated with a 50 ohm load.

The 3D radiation patterns of element#1 and #2 are shown in Fig. 13. In consideration of the orientation and the symmetry among antenna elements, radiation patterns of element#3 and #4 are not shown here. For all the frequencies, the maximum radiation of element#2 is not directly point to element#1 (the maximum radiation nearly points to the null radiation of the other element). This agrees with the aforementioned design principle.

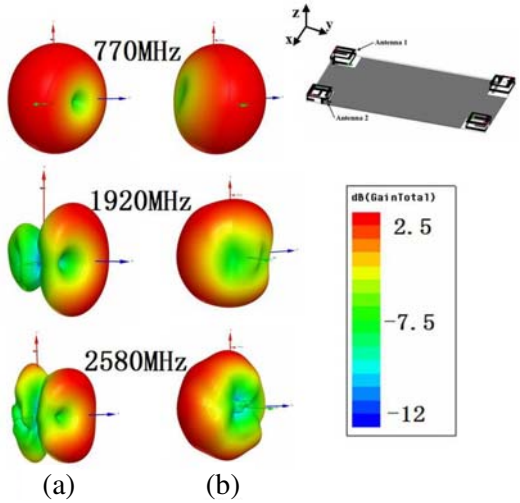

Figure 13. 3D radiation patterns of the proposed antenna: (a) element#1, (b) element#2.

4. CONCLUSION

A dual-band four-element MIMO antenna system for mobile phone application is proposed. By loading the lumped inductor with the antenna elements, the antenna system can cover the GSM1800/1900, UTMS2100 and LTE700/2300/2500 bands with a total size of 140 mm × 70 mm × 6 mm. Without using any specially designed decoupling structures, the measured isolation among antenna elements is higher than 13 dB. Compact size and acceptable performance make it competitive for nowadays handset applications.

ACKNOWLEDGMENT

This work was supported by the Priority Academic Program Development of Jiangsu Higher Education Institutions (PAPD) and Jiangsu Innovation & Entrepreneurship Group Talents Plan.

REFERENCES

1. Song, L. and J. Shen, *Evolved Cellular Network Planning and Optimization for UMTS and LTE*, CRC Press, London, 2011.
2. Dioum, I., A. Diallo, S. M. Farssi, and C. Luxey, "A novel compact dual-band LTE antenna-system for MIMO operation," *IEEE Trans. Antennas Propag.*, Vol. 62, No. 4, 2291–2296, 2014.
3. Yang, L. S., J. P. Fang, and T. Li, "Compact dual-band MIMO antenna system for mobile handset application," *IEICE Trans. on Communications*, Vol. E98-B, No. 12, Dec. 2015.
4. Guo, Y.-X., M. Y. W. Chia, and Z. N. Chen, "Miniature built-in quad-band antennas for mobile handsets," *IEEE Antennas Wireless Propag. Lett.*, Vol. 2, 3–32, 2003.
5. Ban, Y. L., J. H. Chen, J. L. W. Li, and Y. J. Wu, "Small-size printed coupled-fed antenna for eight-band LTE/GSM/UMTS wireless wide area network operation in an internal mobile handset," *IET Microwave, Antennas & Propagation*, Vol. 7, No. 6, 399–407, 2013.
6. Ban, Y.-L., Z.-X. Chen, Z. Chen, K. Kang, and J. L.-W. Li, "Decoupled closely spaced heptaband antenna array for WWAN/LTE smartphone applications," *IEEE Antennas Wireless Propag. Lett.*, Vol. 13, 31–34, 2014.
7. Shoaib, S., I. Shoaib, N. Shoaib, X. D. Chen, and C. G. Parini, "Design and performance study of a dual-element multiband printed monopole antenna array for MIMO terminals," *IEEE Antennas Wireless Propag. Lett.*, Vol. 13, 329–332, 2014.
8. Zeng, Q. H., Y. Yao, S. H. Liu, J. S. Yu, P. Xie, and X. D. Chen, "Tetraband small-size printed strip MIMO antenna for mobile handset application," *International Journal of Antennas and Propagation*, Vol. 2012, Article ID 320582, 2012.
9. Lee, B., F. J. Harackiewicz, and H. Wi, "Closely mounted mobile handset MIMO antenna for LTE13 band application," *IEEE Antennas Wireless Propag. Lett.*, Vol. 13, 31–34, 2014.
10. Yang, C., Y. Yao, J. S. Yu, and X. D. Chen, "Novel compact multiband MIMO antenna for mobile terminal," *International Journal of Antennas and Propagation*, Vol. 2012, Article ID 691681, 2012.
11. Blanch, S., J. Romeu, and I. Corbella, "Exact representation of antenna system diversity performance from input parameter description," *Electron. Lett.*, Vol. 39, No. 9, 705–707, 2003.
12. Qualcomm Corp., San Diego, CA, "Diversity antenna design guide-lines," *Tech. Rep. 80-V8782-5 Rev. B*, Jan. 2006.
13. Vaughan, R. G. and J. B. Andersen, "Antenna diversity in mobile communications," *IEEE Trans. Veh. Technol.*, Vol. 36, No. 4, 149–172, 1987.
14. Cihangir, A., F. Ferrero, G. Jacquemod, P. Brachat, and C. Luxey, "Neutralized coupling elements for MIMO operation in 4G mobile terminals," *IEEE Antennas Wireless Propag. Lett.*, Vol. 13, 141–144, 2014.